Supporting Information

Sulfate Radical–Mediated Methane Conversion to C-C and C-S Products in Water

Mujing Huang,†[a] Fanxun Lv,†[a] Yi Lv,[a] Jiajun Yan [a] and Chenlu Xie *[a, b]

[a] M. Huang, F. Lv, Y. Lv, Prof. J. Yan, Prof. C. Xie

School of Physical Science and Technology, ShanghaiTech University, Shanghai, 201210, China

E-mail: xiechl@shanghaitech.edu.cn

[b] Prof. C. Xie

Shanghai Key Laboratory of High-Resolution Electron Microscopy, ShanghaiTech University, Shanghai, 201210, China

† These authors contributed equally to this work.

Experimental section

Chemicals and materials

Potassium persulfate ($K_2S_2O_8$) (≥99.99%), Sodium methyl sulfate (>98.0%), Dimethyl sulfone (≥99%), Methanesulfonic acid (≥98%), Acetic acid (≥99.7%), Sodium ethyl sulfate (≥98%), Dioxane (≥99.5%) and 5,5-dimethyl-1-pyrroline N-oxide (DMPO) (≥97%) were purchased from Shanghai Aladdin Biochemical Technology Co. CH_4 (99.9%), Ar (99.999%), O_2 (99.999%), CO (99.9%), C_2H_6 (99.99%), $^{13}CH_4$ (^{13}C enrichment >99% atom) were purchased from Wen Dong (Shanghai) Chemical Co. D_2O (99.9%D) was purchased from Energy Chemical Co. Dimethyl sulfoxide (DMSO) (≥99.9%) and Acetone (≥99.5%) were purchased from Sinopharm Chemical Reagent Co. All chemicals and gases were used as received.

Photochemical CH_4 functionalization measurements

In a typical experiment, photochemical reactions were conducted in a 250 mL high-pressure reactor (SenLong, LC250) equipped with a sapphire window for light irradiation (Figure S2). The reactor was charged with 100 mL of 50 mM $K_2S_2O_8$ aqueous solution and purged with Ar (99.999%) to remove the air. Subsequently, CH_4 (99.9%) was introduced to a final pressure of 2.5 MPa. The reaction mixture was irradiated with a 365 nm UV LED lamp (Perfectlight, PLS-LED100C) under continuous stirring at 25±4 °C.

Gas-phase products were analyzed using a gas chromatograph (GC, Agilent 8890) equipped with a flame ionization detector (FID) and a thermal conductivity detector (TCD). Liquid-phase products were quantified by ^1H NMR (Bruker 400 MHz). For NMR analysis, 450 μL of the reaction solution was mixed with 50 μL D_2O containing 0.04 wt% DMSO (δ = 2.72 ppm) as internal standard. Water suppression was applied during acquisition. The concentrations of the products were determined by comparing the area of their ^1H NMR signals to calibration curves. These curves were prepared using pure samples of each chemical (Figure S3).

The liquid product selectivity and CH_4 conversion were calculated as follows:

$$\text{Liquid product selectivity (\%)} = \frac{mol_{total\ formed\ liquid\ products}}{mol_{total\ formed\ products}} \times 100\%$$

$$CH_4 \text{ conversion (\%)} = \frac{mol_{total\ formed\ products}}{mol_{initial\ CH_4}} \times 100\%$$

The initial CH_4 amount in the system is calculated according to the following equation (V is the volume of the headspace of the reactor, R is the gas constant):

$$mol_{initial\ CH_4} = \frac{P_{CH_4} \times V}{R \times T(298K)}$$

Please note that the CH_4 conversion reported in Figure 4b was determined under flow mode conditions without collecting the effluent gas. Thus, the actual CH_4 conversion would be higher.

CH_4 functionalization in a photochemical flow reactor

The continuous-flow photochemical conversion of CH_4 was conducted in a custom-built photochemical flow reactor (MICROFLU V6G, Figure S15). An aqueous $K_2S_2O_8$ solution (50 mM) and CH_4 (0.1 MPa) were premixed in a microfluidic device to generate a uniform stream of gas bubbles in the liquid. This gas-liquid mixture was then pumped into an 18 mL reaction chip. The reactor was sandwiched between two 365 nm LED panels (252 0.5 W LEDs on each panel) to ensure uniform irradiation. The reaction temperature was maintained at 25 °C by flowing aqueous ethylene glycol through the central jacket within the reaction chip, and the residence time was controlled by adjusting the gas and liquid flow rates. The two LED panels were cooled with another stream of aqueous ethylene glycol flown through aluminum jackets. Liquid products were collected at the reactor outlet and quantified by ^{1}H NMR, while gaseous products were quantified by GC.

Products analysis using isotope-labeled $^{13}CH_4$

Isotope-labeling experiments were performed with pure $^{13}CH_4$ in the photochemical flow reactor. A 50 mM $K_2S_2O_8$ aqueous solution and 0.1 MPa $^{13}CH_4$

were introduced into the 18 mL reaction chip. The reactor was then irradiated with 365 nm LED lamps for 30 min. After irradiation, the reaction mixture was analyzed using a Bruker 400 MHz NMR spectrometer, and ^{1}H NMR, ^{13}C NMR and HSQC (two-dimensional ^{1}H-^{13}C heteronuclear single quantum correlation spectroscopy) spectra were collected (Figure S5, Figure S6 and Figure 1e).

Electrospray ionization mass spectrometry (ESI-MS) analysis

Excess inorganic salts (mainly K_2SO_4) in the sample needed to be removed from the reaction solution before ESI-MS analysis. A 50 mL aliquot of the solution was concentrated by heating to remove most of the water. Dioxane was then added to the concentrated residue to precipitate the inorganic salts until no crystals were observed. Finally, 100 μL of sample of the clear supernatant was collected and diluted with CH_3OH. The resulting solution was analyzed by high-resolution mass spectrometry (Thermo Fisher) equipped with an electrospray ionization source. It is worth noting that because the sample preparation involves a heating step, only non-volatile products with boiling points higher than water can be analyzed, such as methanesulfonic acid (CH_3SO_3H) and methyl bisulfate (CH_3SO_4H).

Determination of $K_2S_2O_8$ concentration

The residual $K_2S_2O_8$ concentration after the photochemical reactions was determined using an iodometric method[1] with UV–Vis spectroscopy. A KI stock solution was prepared by dissolving 20 g KI and 1 g $NaHCO_3$ in 200 mL deionized water, where the $NaHCO_3$ was added to prevent the oxidation of KI. For each measurement, 0.05 mL of the reaction solution was mixed with 2.45 mL of the KI stock solution. The absorbance of the mixture was then measured at 346 nm on a UV–Vis spectrometer (PerkinElmer, Lambda 265). The $K_2S_2O_8$ concentration was calculated by comparing the absorbance value to a calibration curve prepared from standard solutions (Figure S7b).

Electron paramagnetic resonance (EPR) measurement

EPR measurements were conducted at room temperature using Bruker EMXplus spectrometer. For a typical experiment, 100 mM DMPO and 50 mM $K_2S_2O_8$ were mixed in either H_2O or DMSO. This mixture bubbled with CH_4 or Ar for 30 min. Subsequently, the solution was transferred to a quartz EPR capillary and irradiated with a 365 nm LED light source. EPR spectra were recorded immediately upon irradiation.

In situ Fourier transform infrared spectroscopy (FTIR) measurement

The FTIR spectra were recorded on a Bruker VERTEX 70 FTIR spectrometer. The reaction mixture was loaded into the sample cell, and a stream of humidified CH_4 gas was continuously introduced into the system for 30 min. Spectra were collected at a resolution of 2 cm^{-1} with 64 scans per spectrum. The evolution of the reaction was monitored continuously over a 30-minute period under light irradiation.

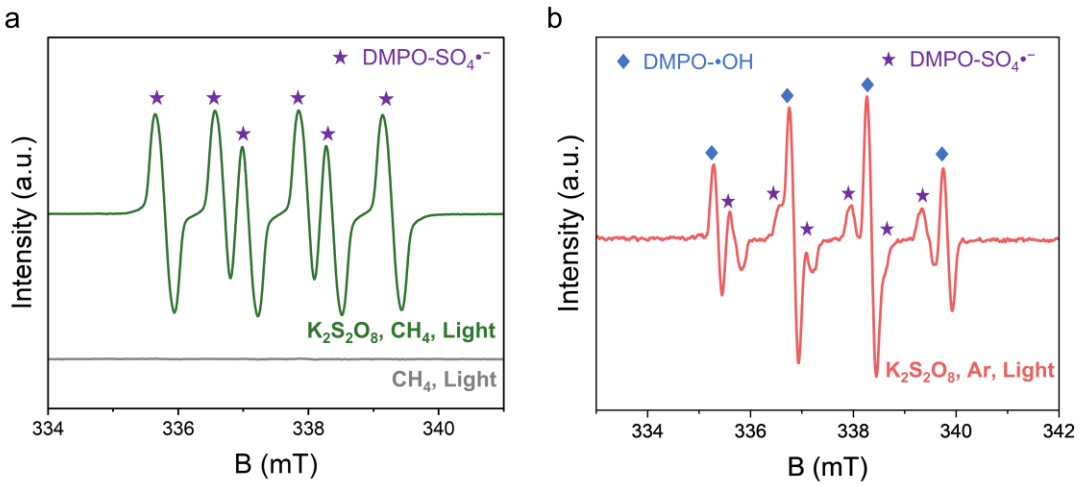

Figure S1. (a), EPR spectra of $SO_4^{\bullet -}$ in DMSO. Green: with $K_2S_2O_8$; grey: without $K_2S_2O_8$. (b), EPR spectra of $K_2S_2O_8$ bubbled with Ar.

a $SO_4^{\bullet-} + SO_3^{2-} \longrightarrow SO_4^{2-} + SO_3^{\bullet-}$

b

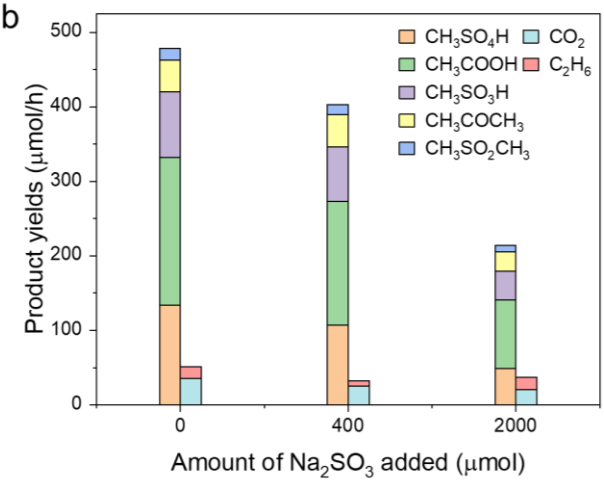

Figure S2. Scavenging experiments using Na_2SO_3 as a selective $SO_4^{\bullet-}$ scavenger. **a**, Reaction mechanism for the scavenging of $SO_4^{\bullet-}$ by SO_3^{2-}.[2] **b**, Variation in product yields with Na_2SO_3 addition.

Reaction conditions: 2.5 MPa CH_4, 100 mL 50 mM $K_2S_2O_8$ aqueous solution, 1 h reaction time, 25 ℃, 365 nm UV LED (80 mW/cm^2).

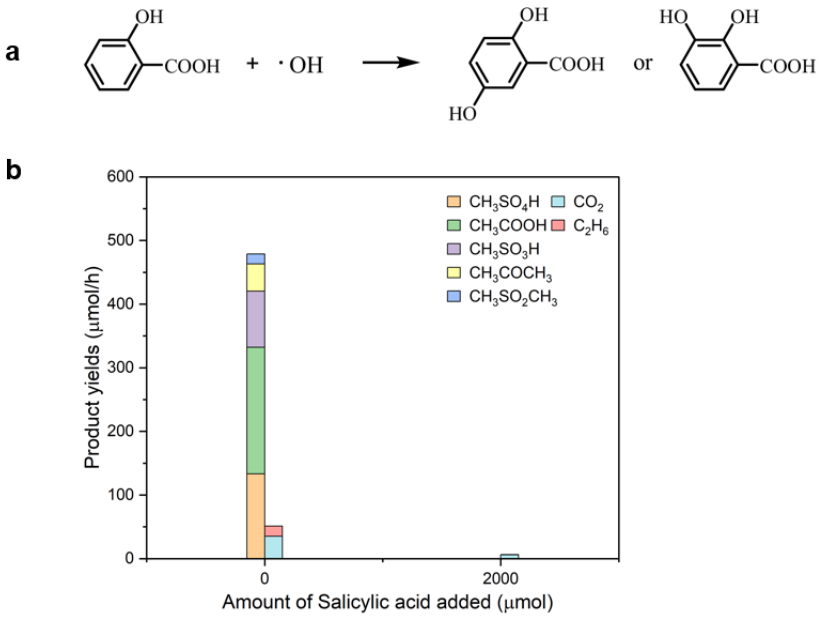

Figure S3. Scavenging experiments using salicylic acid as a selective •OH scavenger.

a, Reaction mechanism for the scavenging of •OH by salicylic acid.[3] **b**, Variation in product yields with salicylic acid addition.

Reaction conditions: 2.5 MPa CH_4, 100 mL 50 mM $K_2S_2O_8$ aqueous solution, 1 h reaction time, 25 ℃, 365 nm UV LED (80 mW/cm^2).

Figure S4. Image of the laboratory-scale high-pressure batch photoreactor used for methane functionalization experiments.

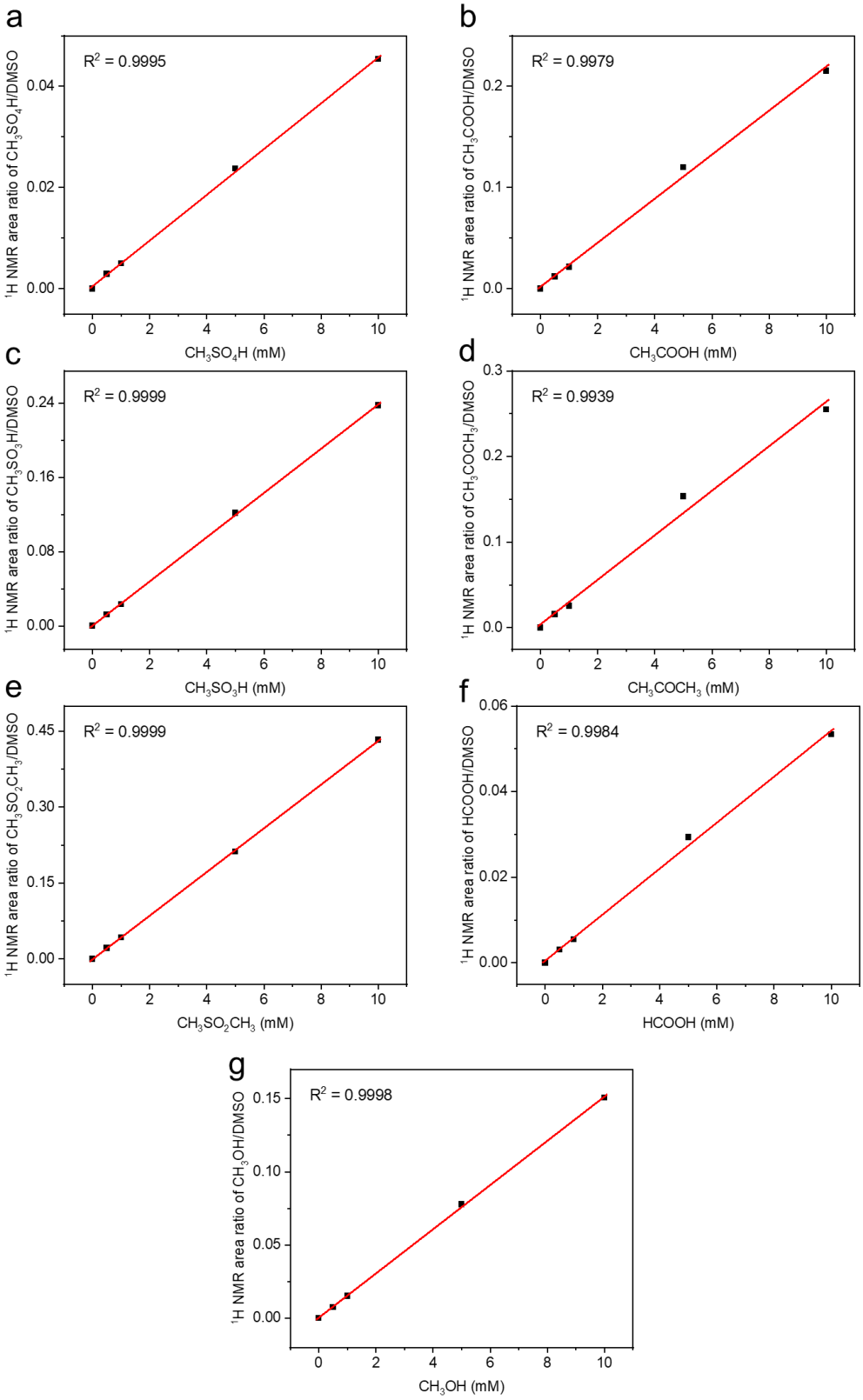

Figure S5. Calibration curves for the quantification of CH_3SO_4H (a), CH_3COOH (b), CH_3SO_3H (c), CH_3COCH_3 (d), $CH_3SO_2CH_3$ (e), HCOOH (f), and CH_3OH (g) by ^1H NMR.

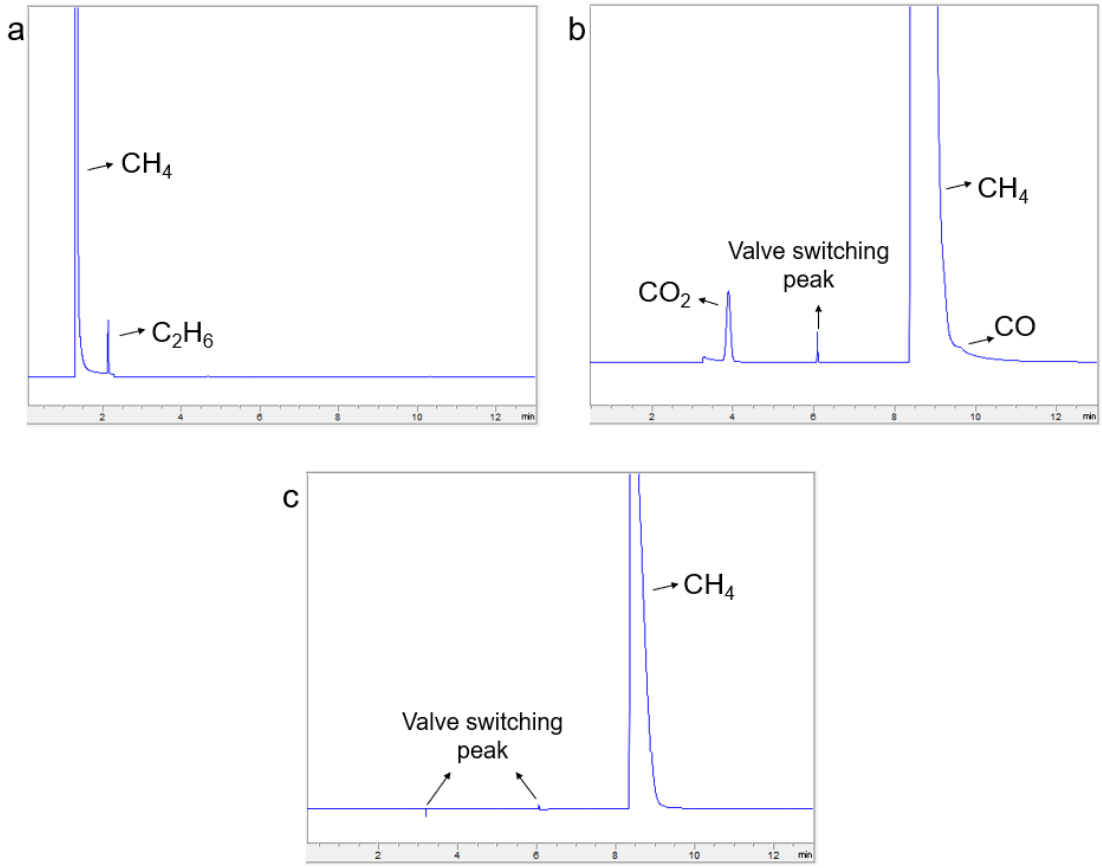

Figure S6. Representative GC spectrum obtained from a typical experiment. **a**, FID signals corresponding to CH_4 and C_2H_6. **b**, FID signal corresponding to CO_2. **c**, TCD signals corresponding to O_2 and N_2.

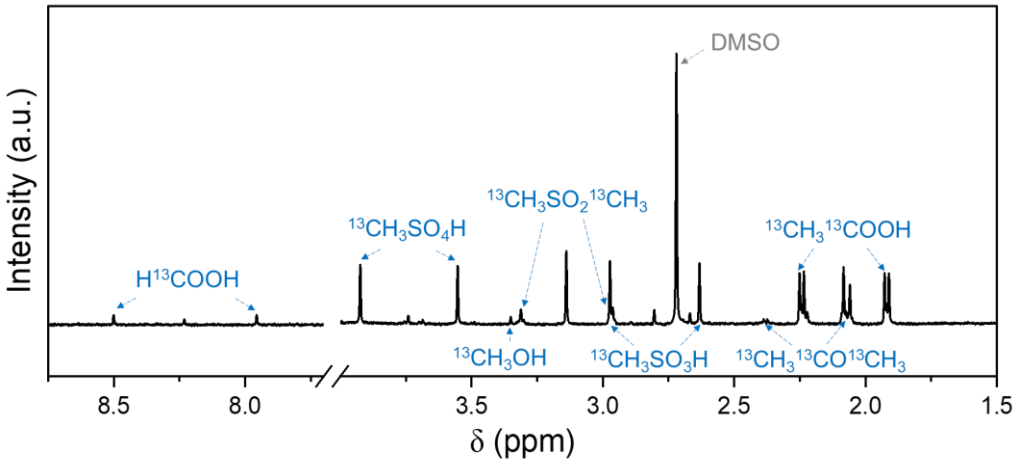

Figure S7. ^{1}H NMR spectrum from the $^{13}CH_4$ isotope-labeling experiment. Reaction condition: $^{13}CH_4$ (0.1 MPa) and $K_2S_2O_8$ (50 mM) in a photochemical flow reactor under UV irradiation.

Note: Minor production of CH_3OH and HCOOH (< 1% combined selectivity) were also observed in the reaction (Table S2).

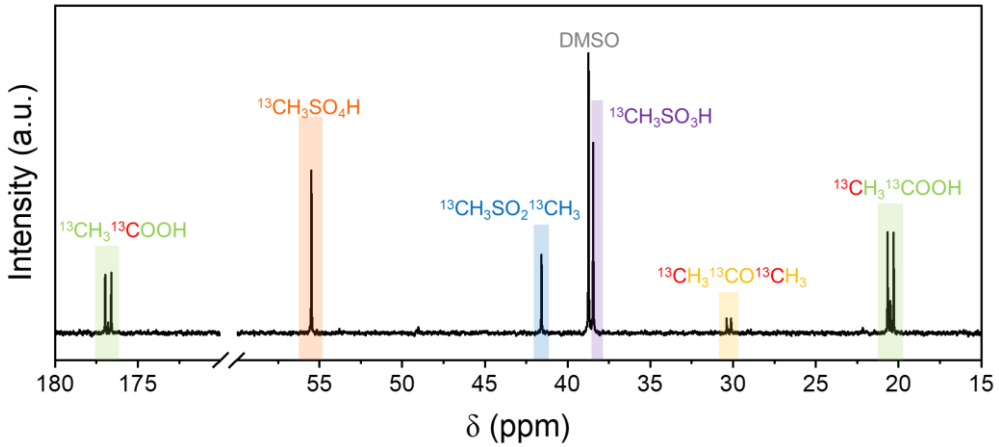

Figure S8. ^{13}C NMR spectrum from the $^{13}CH_4$ isotope-labeling experiment. Reaction condition: $^{13}CH_4$ (0.1 MPa) and $K_2S_2O_8$ (50 mM) in a photochemical flow reactor under UV irradiation.

a $S_2O_8^{2-} + 3I^- \longrightarrow 2SO_4^{2-} + I_3^-$

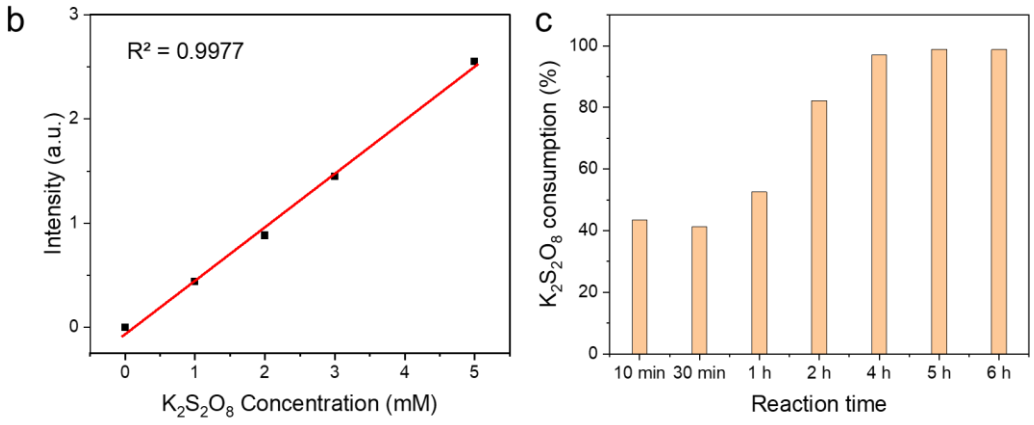

Figure S9. Quantification of $K_2S_2O_8$. **a,** Reaction scheme for the iodometric titration method used to determine $K_2S_2O_8$ concentration.[4] **b,** Calibration curve for the quantification of $S_2O_8^{2-}$ by colorimetric method. **c,** $K_2S_2O_8$ consumption as a function of reaction time. Reaction conditions: 2.5 MPa CH_4, 100 mL 50 mM $K_2S_2O_8$ aqueous solution, reaction temperature: 25 ℃, light source: 365 nm UV LED, 80 mW/cm^2.

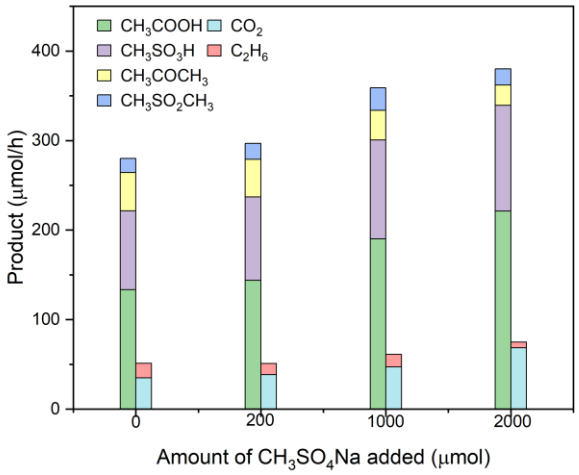

Figure S10. The effect of CH_3SO_4Na addition over the CH_4 functionalization. Reaction conditions: 2.5 MPa CH_4, 100 mL 50 mM $K_2S_2O_8$ aqueous solution, 1 h reaction time, 25 °C, 365 nm UV LED (80 mW/cm^2).

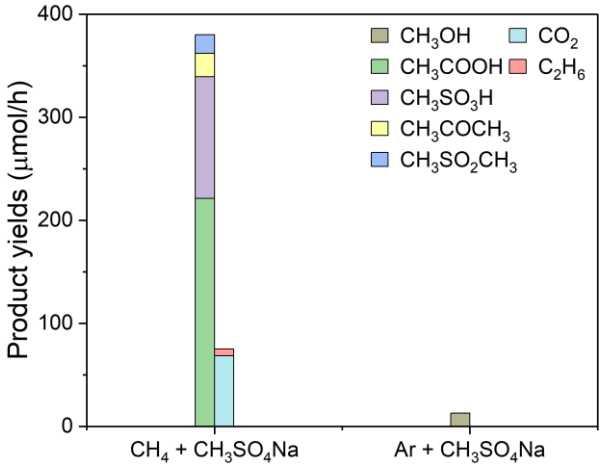

Figure S11. The effect of CH_4 on the conversion of CH_3SO_4H. Reaction conditions: 2.5 MPa CH_4 or Ar, 2 mmol CH_3SO_4Na, 100 mL 50 mM $K_2S_2O_8$ aqueous solution, 1 h reaction time, 25 °C, 365 nm UV LED (80 mW/cm^2).

Note: Only CH_3OH observed in the experiment with Ar, which originates from the hydrolysis of the added CH_3SO_4Na.

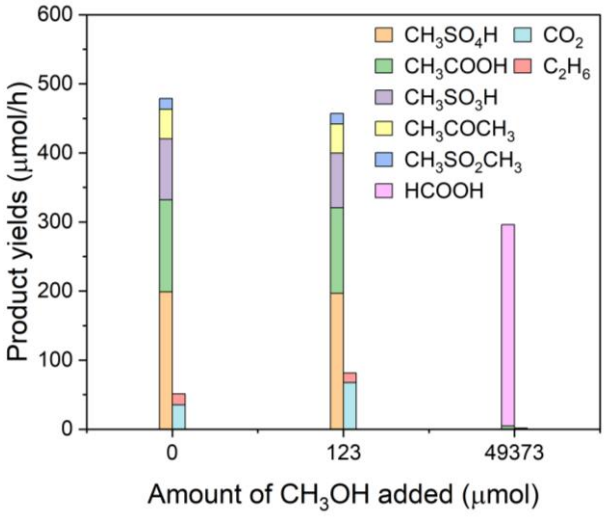

Figure S12. The effect of CH_3OH addition over the CH_4 functionalization. Reaction conditions: 2.5 MPa CH_4, 100 mL 50 mM $K_2S_2O_8$ aqueous solution, 1 h reaction time, 25 °C, 365 nm UV LED (80 mW/cm^2).

Note: The addition of small amounts of CH_3OH have negligible effect on product yields, while excess CH_3OH competes with CH_4, resulting in the formation of HCOOH through CH_3OH overoxidation. This result indicates CH_3OH is not a key intermediate in CH_4 functionalization.

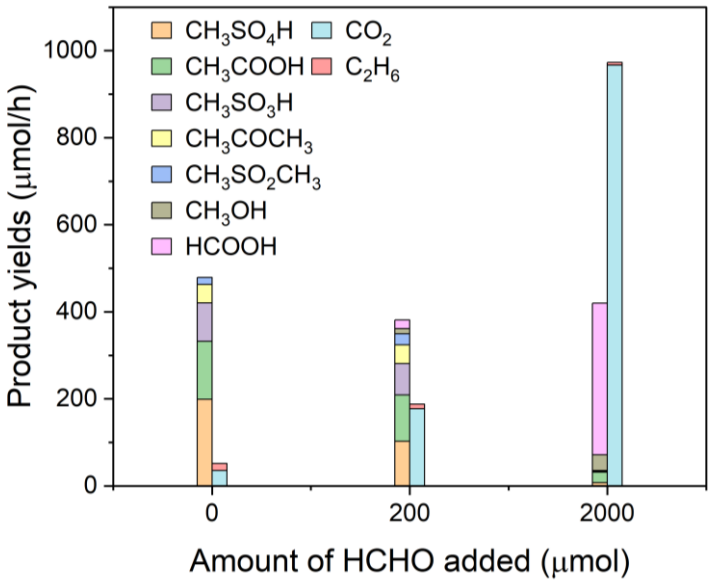

Figure S13. The effect of HCHO addition over the CH_4 functionalization. Reaction conditions: 2.5 MPa CH_4, 100 mL 50 mM $K_2S_2O_8$ aqueous solution, 1 h reaction time, 25 °C, 365 nm UV LED (80 mW/cm^2).

Note: The addition of HCHO leads to overoxidation, resulting in the formation of CO_2 and HCOOH.

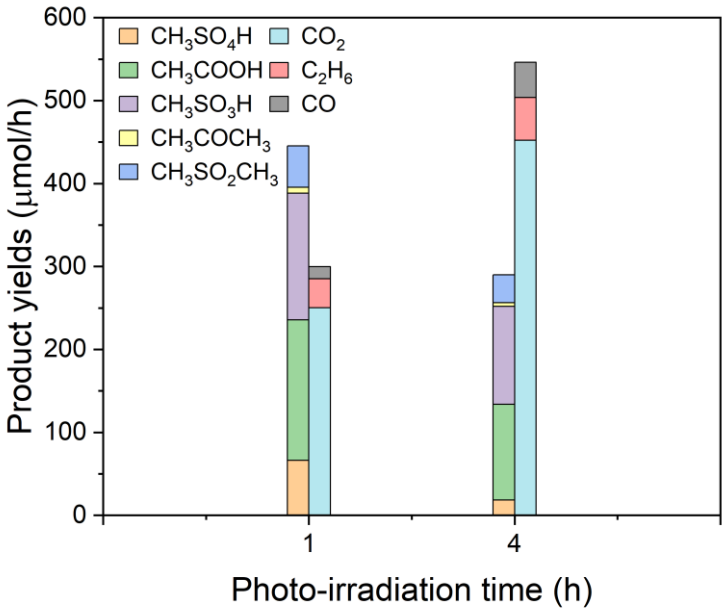

Figure S14. Product yields of CH_4 functionalization in small water volume. Reaction conditions: 2.5 MPa CH_4, 20 mL 250 mM $K_2S_2O_8$ aqueous solution, 25 °C, 365 nm UV LED (80 mW/cm^2).

Note: CO was observed only under conditions with small water volume. Its absence in other experiments is likely due to its low production level.

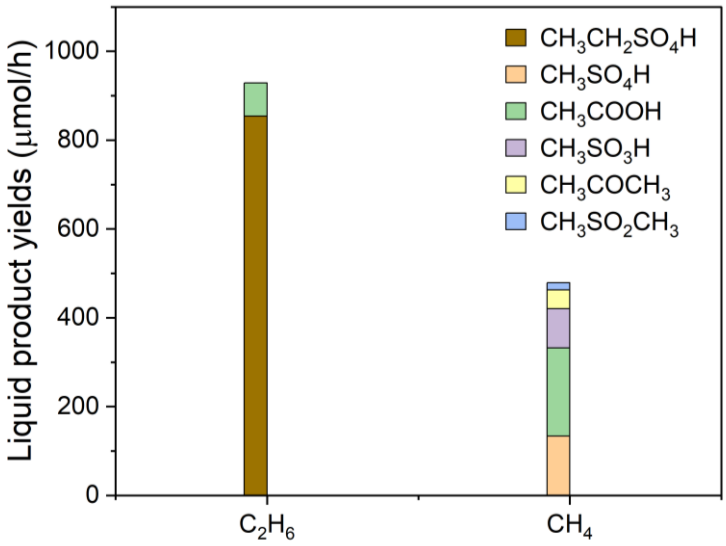

Figure S15. Comparison of CH_4 and C_2H_6 functionalization with $K_2S_2O_8$. Reaction conditions: 2.5 MPa CH_4 or C_2H_6, 100 mL 50 mM $K_2S_2O_8$ aqueous solution, 1 h reaction time, 25 °C, 365 nm UV LED (80 mW/cm^2).

Note: In the C_2H_6 functionalization process, ethyl sulfate was observed as the major product, along with a small amount of CH_3COOH. Ethyl sulfate is presumably generated through the coupling of an ethyl radical with a sulfate radical. In contrast to reactions using CH_4, no C-S product or C-C product observed.

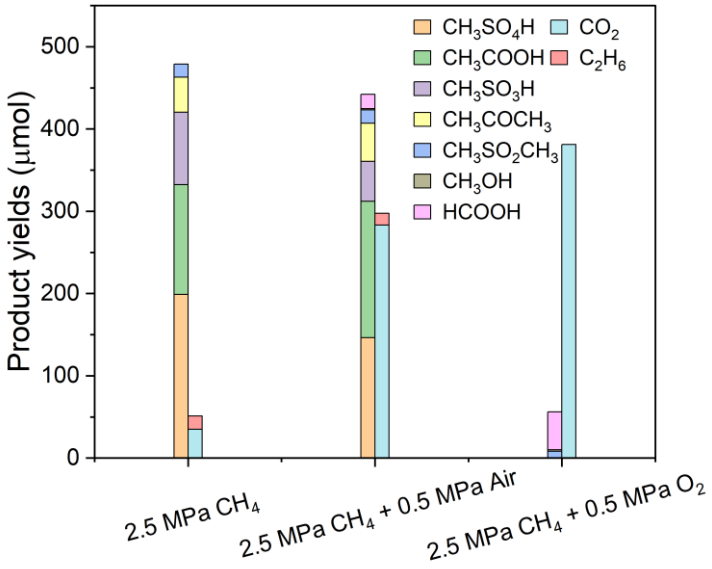

Figure S16. Influence of O_2 on CH_4 functionalization. Reaction conditions: 100 mL 50 mM $K_2S_2O_8$ aqueous solution, 1 h reaction time, 25 °C, 365 nm UV LED (80 mW/cm^2).

Note: Overoxidation becomes more pronounced as the O_2 concentration increases.

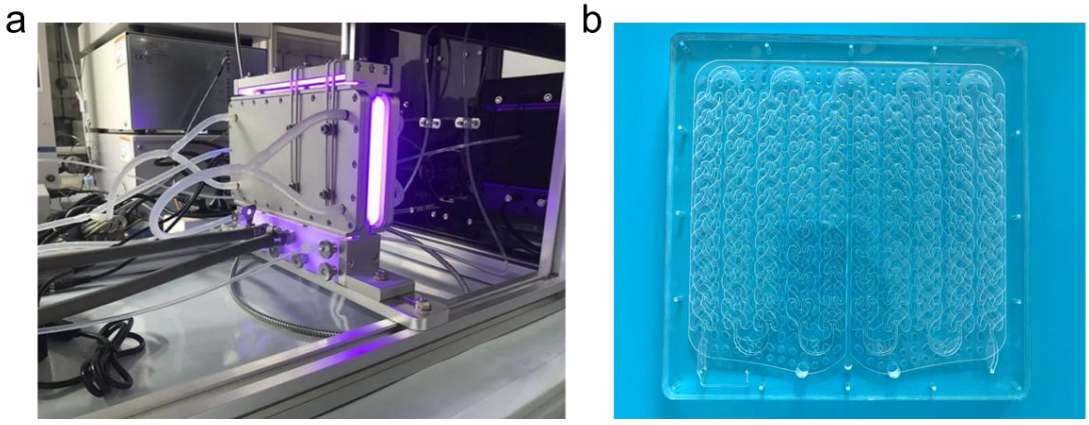

Figure S17. Image of the photochemical flow reactor used for methane functionalization (a) and an 18 mL reaction chip (b).

Table S1. Product yields for sulfate radical–mediated CH_4 functionalization under various reaction conditions

Entry	Reaction condition	Product yields (μmol/h)							All products (μmol/h)	Liquid product Selectivity (%)
		CH_3SO_4H	CH_3COOH	CH_3SO_3H	CH_3COCH_3	$CH_3SO_2CH_3$	CO_2	C_2H_6		
1	$CH_4 + K_2S_2O_8$	188.7	169.2	106.2	50.2	29.6	56.3	3.9	604.0	90.0
2[a]	$Ar + K_2S_2O_8$	0	0	0	0	0	0	0	0	0
3[b]	$CH_4 + H_2O$	0	0	0	0	0	0	0	0	0
4[c]	$CH_4 + K_2S_2O_8$ dark	0	0	0	0	0	0	0	0	0

Reaction conditions (unless otherwise noted): 2.5 MPa CH_4, 150 mL 50 mM $K_2S_2O_8$ aqueous solution, 1 h reaction time, 25 °C, 365 nm UV LED (80 mW/cm^2).

[a] Entry 2: Reaction was conducted under Ar.

[b] Entry 3: Deionized water was used instead of $K_2S_2O_8$ aqueous solution.

[c] Entry 4: Reaction was conducted in the dark.

Table S2. Yields of CH_3OH, HCOOH, and total products in CH_4 functionalization as a function of photo-irradiation time

Entry	Photo-irradiation time (h)	CH_3OH product (μmol)	HCOOH product (μmol)	All products (μmol)
1	0.5	0	0	406.2
2	1	0.5	2.2	532.7
3	2	0.6	1.6	698.8
4	4	2.2	4.5	932.7
5	5	1.4	4.8	946.4

Reaction conditions: 2.5 MPa CH_4, 100 mL 50 mM $K_2S_2O_8$ aqueous solution, 25 °C, 365 nm UV LED (80 mW/cm^2).

Note: At different irradiation times, the selectivity of the minor liquid byproducts (methanol and formic acid) was below 1%.

Table S3. Reaction conditions and MBS production rates compared with reported literatures.

Catalysts	Oxidant/ reactant	Solvent	Temperature (ºC)	CH_4 Pressure (bar)	MBS yields (μmol/h)	Ref.
/[a]	$K_2S_2O_8$	H_2O	25	25	563.9	This work
(V)-oxo dimer	Echem	98% H_2SO_4	25	1	0.2	[5]
Ag_2SO_4	Echem	98% H_2SO_4	25	12.4	0.292	[6]
K_2CrO_4	Echem	98% H_2SO_4	25	1	0.515	[7]
K_2CrO_4	Echem	98% H_2SO_4	25	11	5.9	[7]
$PdSO_4$	Echem and SO_3	oleum with 20 wt% free SO_3	70	34	7.4	[8]
(bpym)$PtCl_2$	SO_3	102% H_2SO_4	220	34	32000	[9]
$HgSO_4$	H_2SO_4	100% H_2SO_4	180	34.5	108000	[10]

[a] Reaction conditions: 2.5 MPa CH_4, 100 mL 50 mM $K_2S_2O_8$ aqueous solution, 1 h reaction time, 25 °C, 365 nm UV LED (320 mW/cm^2).

Table S4. Reaction conditions and MSA production rates compared with reported literatures.

Catalysts	Oxidant/ reactant	Solvent	Temperature (ºC)	CH_4 Pressure (bar)	MSA yields (μmol/h)	Ref.
/[a]	$K_2S_2O_8$	H_2O	25	25	136.9	This work
$HgSO_4$	SO_3	oleum with 30 wt% free SO_3	160	69	266.7	[11]
/	Echem	98% H_2SO_4	140	70	281.3	[12]
/	Echem	oleum with 20-30 wt% free SO_3	70	90	504.5	[13]
/	$K_2S_2O_8$	oleum with 30 wt% free SO_3	90	69	3800	[11]
$RuCl_3$	H_2O_2	oleum with 30 wt% free SO_3	65	45	6100	[14]
/	SO_3	oleum with 36 wt% free SO_3	50	100	3080000	[15]

[a] Reaction conditions: 2.5 MPa CH_4, 100 mL 50 mM $K_2S_2O_8$ aqueous solution, 1 h reaction time, 25 °C, 365 nm UV LED (320 mW/cm^2).

Table S5. Reaction conditions and CH_3COOH production rates compared with reported literatures.

Catalysts	Substrates	Oxidant/ reactant	Solvent	Temperature (ºC)	CH_4 Pressure (bar)	CH_3COOH yields (μmol/h)	Ref.
/[a]	CH_4	$K_2S_2O_8$	H_2O	25	25	208.3	This work
RhFe-MoS_2	CH_4+CO	O_2	H_2O	25	5	0.524	[16]
(Pt/NPW)/TiO_2	CH_4+CO	H_2O	H_2O	20	10	0.972	[17]
Ag/AgCl-WO_{3-X}	CH_4	O_2	H_2O	25	0.01	3.77	[18]
PdO/Pd–WO_3	CH_4	PdO	H_2O	25	1	9.855	[19]
AuFe/ZSM-5	CH_4+CO	O_2	H_2O	80	28	95	[20]
Rh-ZSM-5	CH_4+CO	O_2	H_2O	150	20	142	[21]

[a] Reaction conditions: 2.5 MPa CH_4, 100 mL 50 mM $K_2S_2O_8$ aqueous solution, 1 h reaction time, 25 °C, 365 nm UV LED (320 mW/cm^2).

Supplementary Note 1

To explain the effect of methyl bisulfate (MBS, CH_3SO_4H) addition over the production of methanesulfonic acid (MSA), acetic acid (AA) and acetone, we conducted a simple kinetic model to describe the formation and consumption of key intermediates in the system.

The model is based on a set of elementary steps:

(1) $S_2O_8^{2-}$ (PDS) → 2 $SO_4^{\bullet-}$, k_1

(2) $SO_4^{\bullet-} + H_2O \rightarrow {\bullet}OH + SO_4^{2-} + H^+$, k_2

(3) $SO_4^{\bullet-} + CH_4 \rightarrow {\bullet}CH_3 + SO_4^{2-} + H^+$, k_3

(4) $ {\bullet}OH + CH_4 \rightarrow {\bullet}CH_3 + H_2O$, k_4

(5) $SO_4^{\bullet-} + {\bullet}CH_3 + H^+ \rightarrow CH_3SO_4H$ (MBS), k_5

(6) CH_3SO_4H (MBS) + $ {\bullet}CH_3 \rightarrow CH_3SO_3H$ (MSA) + $CH_3O{\bullet}$, k_6

(7) $CH_3O{\bullet} + {\bullet}OH \rightarrow CH_2O + H_2O$, k_7

(8) $CH_2O + {\bullet}OH \rightarrow CHO{\bullet} + H_2O$, k_8

(9) $CHO{\bullet} + {\bullet}OH \rightarrow CO + H_2O$, k_9

(10) $CO + {\bullet}CH_3 \rightarrow CH_3CO{\bullet}$, k_{10}

(11) $CH_3CO{\bullet} + {\bullet}OH \rightarrow CH_3COOH$, k_{11}

(12) $CH_3CO{\bullet} + {\bullet}CH_3 \rightarrow CH_3COCH_3$, k_{12}

As the radicals have very short lifetime, the steady-state approximation is applied to the radical species [$ {\bullet}CH_3$], [$ {\bullet}OH$], [$SO_4^{\bullet-}$], [$CH_3CO{\bullet}$], [$CH_3O{\bullet}$], [CO], [$CH_2O$], [$CHO{\bullet}$], yielding the following rate equations:

(eq1) $k_6[MBS][{\bullet}CH_3] - k_7[CH_3O{\bullet}][{\bullet}OH] = 0$

(eq2) $k_7[CH_3O{\bullet}][{\bullet}OH] - k_8[CH_2O][{\bullet}OH] = 0$

(eq3) $k_8[CH_2O][{\bullet}OH] - k_9[CHO{\bullet}][{\bullet}OH] = 0$

(eq4) $k_9[CHO{\bullet}][{\bullet}OH] - k_{10}[{\bullet}CH_3][CO] = 0$

(eq5) $k_{10}[{\bullet}CH_3][CO] - k_{11}[CH_3CO{\bullet}][{\bullet}OH] - k_{12}[CH_3CO{\bullet}][{\bullet}CH_3] = 0$

(eq6) $k_3[CH_4][SO_4^{\bullet-}] + k_4[CH_4][{\bullet}OH] - k_5[SO_4^{\bullet-}][{\bullet}CH_3][H^+] - k_6[MBS][{\bullet}CH_3] - k_{10}[{\bullet}CH_3][CO] - k_{12}[CH_3CO{\bullet}][{\bullet}CH_3] = 0$

(eq7) $2k_1[PDS] - k_2[SO_4•^-][H_2O] - k_3[CH_4][SO_4•^-] - k_5[SO_4•^-][•CH_3][H^+] = 0$

(eq8) $k_2[SO_4•^-][H_2O] - k_4[CH_4][•OH] - k_7[•OH][CH_3O•] - k_8[CH_2O][•OH] - k_9[CHO•][•OH] - k_{11}[CH_3CO•][•OH] = 0$

Also, the formation rate of MSA is denoted as R(MSA), which can be described as:

(eq9) $R(MSA) = k_6[MBS][•CH_3]$

Moreover, the formation rate of CH_3COOH and CH_3COCH_3 could be described as:

(eq10) $R(CH_3COOH) = k_{11}[CH_3CO•][•OH]$

(eq11) $R(CH_3COCH_3) = k_{12}[CH_3CO•][•CH_3]$

where k_1, k_2, k_3, k_4, k_5, k_6, k_7, k_8, k_9, k_{10}, k_{11}, and k_{12} are all constants, $[CH_4]$, [MBS], $[H_2O]$, [PDS], $[H^+]$ are constants, and $[•CH_3]$, [•OH], $[CH_3CO•]$ are variables that we need to solve.

Based on the above equations (eq1) to (eq9), we can solved R(MSA), which can be expressed in terms of constants and fixed concentrations:

(eq12) $R(MSA) = \frac{12B-(6A+Bk_1[PDS])+\sqrt{(6A+Bk_1[PDS])^2+24ABk_1[PDS]}}{2}$,

where $A=k_2[H_2O] + k_3[CH_4]$, $B=k_6[MBS]k_5[H^+]$ were constants.

From rate equation (eq1) to (eq4), we have this simple relationship:

(eq13) $R(MSA) = k_{11}[CH_3CO•][•OH] + k_{12}[CH_3CO•][•CH_3]$

According to (eq12), the formation rate of MSA is predicted to increase as the PDS concentration increases. Similarly, the addition of external MBS should also lead to increase of MSA formation. These predictions are consistent with our experimental results in Figure 3b. Moreover, according to (eq13) and elementary step (6), an increase in MBS leads to a decrease in $•CH_3$ concentration, thus would lower the rate for CH_3COCH_3 as shown in (eq10). However, since R(MSA) would increase, the formation rate of CH_3COOH must also increase, as shown by (eq13).

CO can originate not only from the oxidation of $CH_3O•$ but also from the direct oxidation and dehydrogenation of $•CH_3$. To account for this possibility, we developed

an additional kinetic model to explained the effect of CO addition on CH_3COOH and CH_3COCH_3 formation rate. To simplify this system, we assume •OH radical is the only species to active CH_4 and therefore only considered reactions involving •OH radicals.

i. $\bullet OH + CH_4 \rightarrow \bullet CH_3 + H_2O$, k_1

ii. $CO + \bullet CH_3 \rightarrow CH_3CO\bullet$, k_2

iii. $CH_3CO\bullet + \bullet OH \rightarrow CH_3COOH$, k_3

iv. $CH_3CO\bullet + \bullet CH_3 \rightarrow CH_3COCH_3$, k_4

The following rate equations are obtained:

(eq i) $k_2[\bullet CH_3][CO] - k_3[CH_3CO\bullet][\bullet OH] - k_4[CH_3CO\bullet][\bullet CH_3] = 0$

(eq ii) $k_1[CH_4][\bullet OH] - k_2[\bullet CH_3][CO] - k_4[CH_3CO\bullet][\bullet CH_3] = 0$

$$[\bullet CH_3] = \frac{k_1[CH_4][\bullet OH]}{k_2[CO]+k_4[CH_3CO\bullet]}$$

Assume $k_2[CO] >> k_4[CH_3CO\bullet]$,

Then, $$[\bullet CH_3] = \frac{k_1[CH_4][\bullet OH]}{k_2[CO]}$$

CH_3COOH formation rate = $k_{11}[CH_3CO\bullet][\bullet OH] = \frac{k_1k_2k_3[\bullet OH]}{k_2k_3+k_1k_4[CH_4]/[CO]}$

CH_3COCH_3 formation rate = $k_4[CH_3CO\bullet][\bullet CH_3] = \frac{{k_1}^2k_4[CH_4]^2[\bullet OH]}{k_2k_3[CO]+k_1k_4[CH_4]}$

In this framework, an increase in CO concentration is expected to promote the formation of CH_3COOH while reducing the formation of CH_3COCH_3, which is also consistent with our results (Figure 3c).

Supplementary references

1 Y. Huang, J. Zou, J. Lin, H. Yang, M. Wang, J. Li, W. Cao, B. Yuan and J. Ma, *Environmental Science & Technology* 2023, **57**, 18420–18432.

2 T. N. Das, *The Journal of Physical Chemistry A* 2001, **105**, 9142–9155.

3 L. Luo, Z. Gong, Y. Xu, J. Ma, H. Liu, J. Xing and J. Tang, *J. Am. Chem. Soc.* 2022, **144**, 740–750.

4 L. Dai, J. Xu, J. Lin, L. Wu, H. Cai, J. Zou and J. Ma, *Chemosphere* 2021, **272**, 128577.

5 J. Deng, S.-C. Lin, J. Fuller, J. A. Iñiguez, D. Xiang, D. Yang, G. Chan, H. M. Chen, A. N. Alexandrova and C. Liu, *Nat. Commun.* 2020, **11**, 3686.

6 D. Xiang, J. A. Iñiguez, J. Deng, X. Guan, A. Martinez and C. Liu, *Angew. Chem. Int. Ed.* 2021, **60**, 18152–18161.

7 J. Deng, S.-C. Lin, J. T. Fuller III, B. Zandkarimi, H. M. Chen, A. N. Alexandrova and C. Liu, *Angew. Chem. Int. Ed.* 2021, **60**, 26630–26638.

8 M. E. O'Reilly, R. S. Kim, S. Oh and Y. Surendranath, *ACS Central Science* 2017, **3**, 1174–1179.

9 R. A. Periana, D. J. Taube, S. Gamble, H. Taube, T. Satoh and H. Fujii, *Science* 1998, **280**, 560–564.

10 R. A. Periana, D. J. Taube, E. R. Evitt, D. G. Löffler, P. R. Wentrcek, G. Voss and T. Masuda, *Science* 1993, **259**, 340–343.

11 N. Basickes, T. E. Hogan and A. Sen, *J. Am. Chem. Soc.* 1996, **118**, 13111–13112.

12 J. Britschgi, M. Bilke, W. Schuhmann and F. Schüth, *ChemElectroChem* 2022, **9**, e202101253.

13 J. Britschgi, W. Kersten, S. R. Waldvogel and F. Schüth, *Angew. Chem. Int. Ed.* 2022, **61**, e202209591.

14 S. Mukhopadhyay and A. T. Bell, *Angew. Chem. Int. Ed.* 2003, **42**, 2990–2993.

15 C. Díaz-Urrutia and T. Ott, *Science* 2019, **363**, 1326–1329.

16 J. Mao, H. Liu, Y. Li, M. Gao, Y. Zhang, Y. Song, M. Zhang, G. Xu, W. Zhou, L. Yu, X. Cui and D. Deng, *J. Am. Chem. Soc.* 2025, **147**, 14530–14540.

17 C. Dong, M. Marinova, K. B. Tayeb, O. V. Safonova, Y. Zhou, D. Hu, S. Chernyak, M. Corda, J. Zaffran, A. Y. Khodakov and V. V. Ordomsky, *J. Am. Chem. Soc.* 2023, **145**, 1185–1193.

18 J. Wang, L. Zhang, D. Zeng, W. Wang, R. Li, T. Jia, B. Cui, H. Chu and W. Wang, *Appl. Catal. B: Environ.* 2023, **337**, 122983.

19 W. Zhang, D. Xi, Y. Chen, A. Chen, Y. Jiang, H. Liu, Z. Zhou, H. Zhang, Z. Liu, R. Long and Y. Xiong, *Nat. Commun.* 2023, **14**, 3047.

20 B. Wu, H. Yin, X. Ma, R. Liu, B. He, H. Li and J. Zeng, *Angew. Chem. Int. Ed.* 2025, **64**, e202412995.

21 J. Shan, M. Li, L. F. Allard, S. Lee and M. Flytzani-Stephanopoulos, *Nature* 2017, **551**, 605–608.